# Analysis of Stress Gradient in Ceramic Film by X-ray Method*

Kenji SUZUKI**, Keisuke TANAKA***
and Yoshihisa SAKAIDA***

The $\sin^2\psi$ diagram taken from a specimen with steep stress gradients beneath the surface shows nonlinearity, because the X-ray penetration depth changes depending on the tilt angle. Stress gradients can be determined from this nonlinearity. Since ceramic materials have deep X-ray penetration depth, the thickness of a ceramic thin film should have a significant effect on the nonlinearity of the $\sin^2\psi$ method. In this paper, we propose a method of X-ray measurement of the stress gradient, which takes into account film thickness under the assumption of linear stress distributions. A 58-$\mu$m-thick silicon nitride film was prepared. The film specimen was polished carefully with diamond slurry to obtain sharp profiles of the X-ray diffraction. To obtain a steep stress gradient, the specimen was bent on a cylinder. The stress distribution estimated by the present method agreed well with the applied bending stress. In conclusion, the stress gradient should be analyzed by the weighted average stress on the basis of the intensity of the diffracted X-rays from the entire thin film, when the thickness is six times larger than the effective X-ray penetration depth.

***Key Words***: Residual Stress, Experimental Stress Analysis, Ceramics, X-ray Stress Measurement, Thin Film, Coating Film

## 1. Introduction

Various coating methods have been developed to improve surface characteristics. In the coating process, residual stress is inevitably introduced into the film due to a mismatch of coefficients of thermal expansions between the coating film and the substrate, and to other mechanisms. Among the various methods used for the measurement of residual stresses, the method based on X-ray diffraction is the most useful. Many X-ray measurements[1]-[7] on thin films and coated films have been reported.

The X-rays penetrate some distance into the specimen. The $\sin^2\psi$ diagram taken from a material that has a steep stress gradient shows nonlinearity, because the X-ray penetration depth changes with the tilt angle $\psi$. Yoshioka et al.[8] proposed the $\cos\psi$ method by which the stress gradient was determined from the nonlinearity in the $\sin^2\psi$ diagram.

In the X-ray stress analysis of the nonlinearity in the diagram, we need the true X-ray penetration depth. We have shown experimentally that the X-ray penetration depth should be equal to the thickness of the specimen[9]. A film whose thickness is six times larger than the effective X-ray penetration depth can be regarded as being thick enough, and the penetration depth can be considered infinite.

If a ceramic film is not thick enough, the film thickness should be taken into account. Sasaki et al.[10]-[12] calculated the stress gradient by using the weighted average stress from the surface to the depth where the ratio of X-ray diffraction intensity to the entire diffraction intensity became $1-1/e$. On the basis of our previous experience, we conclude that the diffraction intensity from the entire film enable an accurate determination of the stress gradient. It is necessary to discuss the definition of penetration depth for obtaining the weighted average stress.

In this paper, we propose the theory and the

* Received 26th September, 1997. Japanese original: Trans. Jpn. Soc. Mech. Eng., Vol. 63, No. 610, A (1997), p. 1243-1248 (Received 21st August, 1996)
** Faculty of Education, Niigata University, 8050 Igarashi-2-no-cho, Niigata 950-2181, Japan
*** Faculty of Engineering, Nagoya University, Furoh-cho, Chikusa-ku, Nagoya 464-8601, Japan
**** Japan Fine Ceramics Center, 2-4-1 Rokuno, Atsuta-ku, Nagoya 456-0023, Japan

analytical method for determining the stress gradient of thin films. We solve the problem of penetration depth experimentally, and discuss the effect of film thickness on the nonlinearity of the $\sin^2\psi$ diagram.

## 2. Analysis Method

### 2.1 X-ray stress analysis of thin film

The coordinate system is defined as shown in Fig. 1. The stress state is assumed to be plane stress. The relationship between diffraction angle $2\theta_{\phi\psi}$ and stresses is given by

$$2\theta_{\phi\psi}=-\frac{2(1+\nu)}{E}\tan\theta_0(\sigma_1\cos^2\phi+\sigma_2\sin^2\phi)\sin^2\psi+\frac{2\nu}{E}\tan\theta_0(\sigma_1+\sigma_2)+2\theta_0, \quad (1)$$

where $\sigma_1$ and $\sigma_2$ are in-plane principal stresses and $2\theta_0$ is the diffraction angle of the stress-free material.

The intensity $I(x)$ of the incident X-ray decreases with path length $x$, and is written as

$$-\frac{dI}{I}=\mu dx. \quad (2)$$

The integration of Eq.(2) gives

$$I=I_0\exp(-\mu x), \quad (3)$$

where $I_0$ is the intensity of the incident X-ray, and $\mu$ is the linear absorption coefficient of the ceramic film. The effective X-ray penetration depth $T$ is defined[13] as the depth where the ratio $I/I_0$ becomes $1/e$. In the iso-inclination method, $T$ is given by

$$T=\frac{\sin^2\theta-\sin^2\psi}{2\mu\sin\theta\cos\phi}. \quad (4)$$

Since the diffraction intensity decreases with increasing the penetration distance of the X-ray, the measured diffraction angle, $\langle 2\theta_{\phi\psi}\rangle$, is represented by the weighted average from the surface to the film thickness $t$. Thus, $\langle 2\theta_{\phi\psi}\rangle$ becomes

$$\langle 2\theta_{\phi\psi}\rangle=\frac{\int_0^t 2\theta_{\phi\psi}I(z)dz}{\int_0^t I(z)dz}=\frac{\int_0^t 2\theta_{\phi\psi}\exp(-z/T)dz}{\int_0^t\exp(-z/T)dz}. \quad (5)$$

Equation (1) is rewritten as

$$\langle 2\theta_{\phi\psi}\rangle=-\frac{2(1+\nu)}{E}\tan\theta_0(\langle\sigma_1\rangle\cos^2\phi+\langle\sigma_2\rangle\sin^2\phi)\sin^2\psi+\frac{2\nu}{E}\tan\theta_0\cdot(\langle\sigma_1\rangle+\langle\sigma_2\rangle)+2\theta_0. \quad (6)$$

Now, we assume that the stress distribution is linear along the $z$-coordinate through the depth of the film

$$\sigma_1=\sigma_{10}+A_1z,\qquad \sigma_2=\sigma_{20}+A_2z, \quad (7)$$

where $\sigma_{10}$ and $\sigma_{20}$ are the stresses on the surface, and $A_1$ and $A_2$ are their gradients. By substituting Eq. (7) into Eq.(6), we have

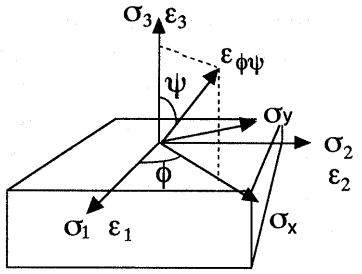


Fig. 1 Coordinate system

$$\langle\sigma_1\rangle=\frac{\int_0^t\sigma_1I(z)dz}{\int_0^t I(z)dz}=\frac{\int_0^t(\sigma_{10}+A_1z)\exp(-z/T)dz}{\int_0^t\exp(-z/T)dz}=\sigma_{10}+A_1\left(T-\frac{t}{e^{t/T}-1}\right), \quad (8)$$

and we obtain a similar equation for the weighted average stress $\langle\sigma_2\rangle$. The weighted average stresses for the thin film are written as

$$\langle\sigma_1\rangle=\sigma_{10}+A_1W_t,\qquad \langle\sigma_2\rangle=\sigma_{20}+A_2W_t, \quad (9)$$

where

$$W_t=T-\frac{t}{e^{t/T}-1}. \quad (10)$$

The $W_t$ value includes the film thickness $t$ explicitly, and is the weighted coefficient for the thin film. For case of thickness $t$ much larger than $T$, $W_t$ is equal to the effective X-ray penetration depth $T$. In the case of thin films, the weighted coefficient $W_t$ necessary for the calculation of the stress gradient. The stress gradient should be calculated using the diffraction intensity from the entire film.

Substituting Eq.(9) into Eq.(6) yields

$$\langle 2\theta_{\phi\psi}\rangle=-\frac{2(1+\nu)}{E}\tan\theta_0[(\sigma_{10}+A_1W_t)\cos^2\phi+(\sigma_{20}+A_2W_t)\sin^2\phi]\sin^2\psi+\frac{2\nu}{E}\tan\theta_0[\sigma_{10}+\sigma_{20}+(A_1+A_2)W_t]+2\theta_0. \quad (11)$$

By denoting the diffraction angles measured in the directions of $\phi=0°$ and $\phi=90°$ as $\langle 2\theta_{\phi=0\psi}\rangle$ and $\langle 2\theta_{\phi=90\psi}\rangle$, the following equations are obtained from the sum of and the difference between $\langle 2\theta_{\phi=0\psi}\rangle$ and $\langle 2\theta_{\phi=90\psi}\rangle$:

$$\langle 2\theta_{\phi=0\psi}\rangle+\langle 2\theta_{\phi=90\psi}\rangle=\alpha[\sigma_{10}+\sigma_{20}+(A_1+A_2)W_t]+\beta[\sigma_{10}+\sigma_{20}+(A_1+A_2)W_t]+4\theta_0$$

$$\langle 2\theta_{\phi=0\psi}\rangle-\langle 2\theta_{\phi=90\psi}\rangle=\alpha[\sigma_{10}-\sigma_{20}+(A_1-A_2)W_t], \quad (12)$$

where $\alpha$ and $\beta$ are

$$\alpha=-\frac{2(1+\nu)}{E}\tan\theta_0\sin^2\psi,\qquad \beta=\frac{4\nu}{E}\tan\theta_0. \quad (13)$$

To analyze the stress distributions, we must obtain the $\sin^2\psi$ diagrams in two directions, $\phi=0°$ and $\phi=90°$, and from the $\sin^2\psi$ diagrams we determine optimum values of parameters $\sigma_{10}$, $\sigma_{20}$, $A_1$ and $A_2$.

### 2.2 Determination method of stress gradients

In this section, we derive the determination method of stress distributions, $\sigma_{10}$, $\sigma_{20}$, $A_1$, $A_2$ and $\theta_0$, using the $\sin^2\psi$ diagrams measured in two directions, $\phi=0°$ and $\phi=90°$. To simplify the equations, we replace the parameters with $c_i$ as

$$\begin{aligned} c_1&=\sigma_{10}+\sigma_{20}\\ c_2&=A_1+A_2\\ c_3&=\theta_0\\ c_4&=\sigma_{10}-\sigma_{20}\\ c_5&=A_1-A_2, \end{aligned} \tag{14}$$

and denote the left-hand terms of Eq.(12) using $Y$ and $Z$:

$$\begin{aligned} Y&=\langle 2\,\theta_{\phi=0\psi}\rangle+\langle 2\,\theta_{\phi=90\psi}\rangle\\ Z&=\langle 2\,\theta_{\phi=0\psi}\rangle-\langle 2\,\theta_{\phi=90\psi}\rangle. \end{aligned} \tag{15}$$

Using Eqs.(14) and (15), Eq.(12) is rewritten as

$$\begin{aligned} Y_j&=(\alpha_j+\beta)c_1+(\alpha_j+\beta)W_tc_2+4\,c_3\\ Z_j&=\alpha_jc_4+\alpha_jW_tc_5, \end{aligned} \tag{16}$$

where the suffix $j$ means the tilt angle $\psi$. We use $y_{\phi=0j}$ and $y_{\phi=90j}$ for measured data, $R_j$ for the error of measured $y_j$ and calculated $Y_j$, and $Q_j$ for the error of measured $y_j$ and calculated $Z_j$. The errors $R_j$ and $Q_j$ are

$$\begin{aligned} R_j&=(\alpha_j+\beta)c_1+(\alpha_j+\beta)W_tc_2+4\,c_3\\ &\quad-(y_{\phi=0j}+y_{\phi=90j})\\ Q_j&=\alpha_jc_4+\alpha_jW_tc_5-(y_{\phi=0j}-y_{\phi=90j}). \end{aligned} \tag{17}$$

In this study, the parameters were determined so as to minimize errors $R$ and $Q$ by the method of least-squares estimation of nonlinear parameters[14]. The relation between errors $R$ and parameters $c_i$ is given by

$$\begin{bmatrix} \sum_{j=1}^{n}(\alpha_j+\beta)^2 & \sum_{j=1}^{n}(\alpha_j+\beta)^2W_t & \sum_{j=1}^{n}4(\alpha_j+\beta)\\ \sum_{j=1}^{n}(\alpha_j+\beta)^2W_t & \sum_{j=1}^{n}(\alpha_j+\beta)^2W_t^2 & \sum_{j=1}^{n}4(\alpha_j+\beta)W_t\\ \sum_{j=1}^{n}4(\alpha_j+\beta) & \sum_{j=1}^{n}4(\alpha_j+\beta)W_t & \sum_{j=1}^{n}4^2 \end{bmatrix} \times \begin{bmatrix} \delta c_1\\ \delta c_2\\ \delta c_3 \end{bmatrix} = \begin{bmatrix} -\sum_{j=1}^{n}(\alpha_j+\beta)R_j\\ -\sum_{j=1}^{n}(\alpha_j+\beta)W_tR_j\\ -\sum_{j=1}^{n}4\,R_j \end{bmatrix}, \tag{18}$$

and the relation for errors $Q$ becomes

$$\begin{bmatrix} \sum_{j=1}^{n}\alpha_j^2 & \sum_{j=1}^{n}W_t\alpha_j^2\\ \sum_{j=1}^{n}\alpha_j^2W_t & \sum_{j=1}^{n}W_t^2\alpha_j^2 \end{bmatrix} \begin{bmatrix} \delta c_4\\ \delta c_5 \end{bmatrix} = \begin{bmatrix} -\sum_{j=1}^{n}\alpha_jQ_j\\ -\sum_{j=1}^{n}W_t\alpha_jQ_j \end{bmatrix}. \tag{19}$$

Solving these equations for $\delta c_1, \delta c_2, \cdots, \delta c_5$, further optimized parameters $c_i'$ are calculated from $\delta c_i$ as follows.

$$\begin{aligned} c_0'&=c_0+\delta c_0\\ c_1'&=c_1+\delta c_1\\ &\vdots\\ c_5'&=c_5+\delta c_5 \end{aligned} \tag{20}$$

Table 1 Mechanical properties and thickness of the test specimen

| Young's modulus $E$ (GPa) | Poisson's ratio $\nu$ | Bulk density (g/cm$^3$) | Bending strength $\sigma_B$ (MPa) | Thickness $t$ ($\mu$m) |
|---|---|---|---|---|
| 320 | 0.27 | 3.23 | 1035 | 58 |

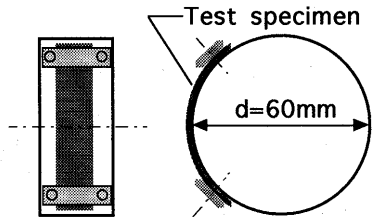


Fig. 2 Bending jig for thin film

Substituting $c_i'$ as new parameters in $c_i$ and repeating the calculation, we finally obtain the optimum parameters.

## 3. Experimental Method

### 3.1 Specimen and bending test

The stress gradient experiment requires a very thin film having high strength for the bending test, as well as a large X-ray penetration depth. In the present experiment, gas-pressure-sintered silicon nitride was used as the test specimen. The mechanical properties and the thickness of the specimen are shown in Table 1. The ceramic thin film was polished carefully to narrow the line broadening; thus we could obtain accurate data at large $\psi$. We removed a 30-$\mu$m-thick laryer from both surfaces of the specimen by polishing with diamond slurry of 6 $\mu$m in diameter, and then removed a 20-$\mu$m-thick layer by lapping with diamond slurry of 2 $\mu$m diameter. The final thickness of the specimen was 58 $\mu$m. The effective X-ray penetration depth of Cu-K$\alpha$ radiation for silicon nitride was 34.7 $\mu$m at $\psi=0°$. The thickness of the specimen was 1.7 times larger than the penetration depth. The thickness of the specimen was appropriate for our experiment.

By bending the specimen on the cylinder, we were able to apply a linear stress distribution to the specimen. The bending jig used is shown in Fig. 2. Both ends of the specimen were fixed on the cylinder with strap plates, and so the known radius of curvature was applied to the specimen. The material of the bending jig was vinyl chloride, which does not diffract X-rays. The specimen with the jig can be held accurately by the holder on the goniometer stage in the directions of $\phi=0°$ and 90°.

The stress-strain relationship for a pure bending plate is given by

$$\varepsilon_1=\frac{y}{r}, \tag{21}$$

where $y$ is the distance from the neutral axis in the thickness direction, and $r$ is the curvature of the neutral plane. During pure bending of a plate, we can assume $\varepsilon_2=0$ and $\sigma_3=0$. Thus, the stress-strain relationships become

$$\varepsilon_1=\frac{1}{E}(\sigma_1-\nu\sigma_2)$$

$$\varepsilon_2=\frac{1}{E}(\sigma_2-\nu\sigma_1)=0 \tag{22}$$

and the stress distributions in the depth direction are given by

$$\sigma_1=\frac{E}{1-\nu^2}\varepsilon_1 \tag{23}$$

$$\sigma_2=\nu\sigma_1. \tag{24}$$

These equations correspond to Eq.(7), and the known values of stress gradients are applied to the thin film specimen. The applied gradients were as follows: $\sigma_{10}=333$ MPa, $\sigma_{20}=90$ MPa, $A_1=-11.5$ MPa/$\mu$m, and $A_2=-3.10$ MPa/$\mu$m.

### 3.2 X-ray stress measurements

The X-ray stress was measured by the fixed plane normal method with the iso-inclination arrangement and the X-ray optics was the parallel beam method. The X-ray conditions are summarized in Table 2. We used the Cu-K$\alpha$ characteristic X-ray, since it has deep X-ray penetration depth. It is preferable that the range of $\sin^2\psi$ be wide, although the measurements at large $\psi$ become inaccurate. The values of $\sin^2\psi$ ranged from 0 to 0.8 within measurement limits, and the increment of $\sin^2\psi$ was 0.05. The diffraction angle was determined from the average of three measurements. The X-ray elastic constants used were the experimental values reported previously[15].

In this experiment, the accuracy of $\psi$ directly influences the accuracy of the stress gradient analysis, so we had to prevent the backlash of the $\psi$-goniometer.

## 4. Results and Discussion

### 4.1 Comparison of experimental results and applied stress

Figure 3 shows the $\sin^2\psi$ diagram of the thin film bent in the jig. The curve in the figure indicates the results of stress gradient analysis in which the effect of film thickness is taken into account. The relationship in the $\sin^2\psi$ diagram shows nonlinearity due to a steep stress gradient of the bent specimen. The analysis agrees well with measured data. The optimized parameters for stress distributions are summarized in Table 3. The analyzed values of the surface stress and the stress gradient correspond very well to the applied values. However, the analyzed value of the surface stress $\sigma_{20}$ does not agree with the applied value. This may be due to the effect of the specimen edge.

Table 2 X-ray conditions for stress measurement

| | |
|---|---|
| Characteristic X-ray | Cu-K$\alpha_1$ |
| Diffraction | 3 2 3 |
| Diffaction angle $2\theta$ | 141.260 deg |
| $\sin^2\psi$ | 0.00 ~ 0.80 |
| Tube voltage | 40 kV |
| Tube current | 30 mA |
| Filter | Ni |
| Divergent angle | 0.64 deg |
| Preset time | 2 sec |
| Scanning speed | 1 deg/min |
| Irradiated area | 4 × 10mm$^2$ |
| Stress constant $S$ | −811 MPa/deg |
| X-ray elastic constant $E$ | 339 GPa |
| X-ray Poisson's ratio $\nu$ | 0.285 |
| Linear absorption factor $\mu$ | 136/cm |

Table 3 Analytical results of bent thin plate

| Stress distribution | | Applied value | Analyzed value |
|---|---|---|---|
| $\sigma_{10}$ | (MPa) | 333 | 392 |
| $\sigma_{20}$ | (MPa) | 90.0 | 201 |
| $A_1$ | MPa/$\mu$m | −11.5 | −14.2 |
| $A_2$ | MPa/$\mu$m | −3.10 | −3.91 |

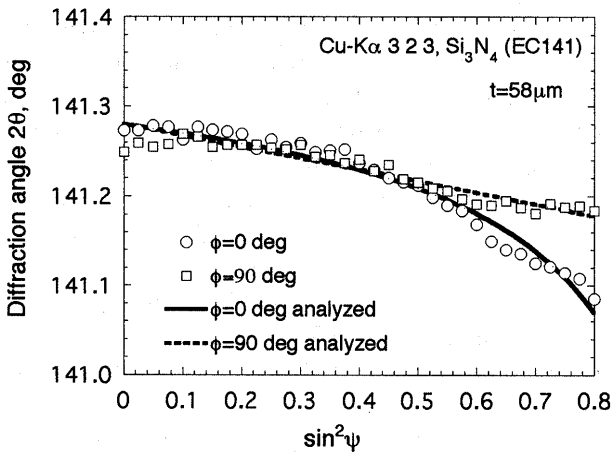


Fig. 3 $2\theta$ vs. $\sin^2\psi$ diagram of bent thin film

From the good agreement between measured and applied values, the weighted coefficient $W_t$ proposed in this study is concluded to be appropriate for the analysis of stress gradient of a thin film. The X-ray stress gradient for a thin film can be calculated by using the X-ray intensity diffracted from the entire thin film. This conclusion is consistent with the case of a bulk plate reported previously[9]. Thus, stress gradient analysis using the weighted coefficient $W_t$ is applicable to both thin films and bulk plates. In the

analysis of the $\sin^2\psi$ diagram of a ceramic coating film showing nonlinearity, analysis using $W_t$ is necessary.

### 4.2 Effect of film thickness

By changing the values of $\sin^2\psi$ from 0 to 0.8, the value of $t/T$ changes from 1.67 to 7.39. The weighted coefficient $W_t$ and the effective penetration depth $T$ change with the $\sin^2\psi$ value. These changes calculated using Eq.(10) for various film thicknesses are shown in Fig. 4. The X-ray penetration depth $T$ decreases with increasing $\sin^2\psi$ value, and then becomes equal to $W_t$. For the case of 58-$\mu$m-thick specimen used in the present experiment, $W_t$ is smaller than $T$ for small values of $\sin^2\psi$ and becomes equal to $T$ at $\sin^2\psi=0.8$. This means that the film thickness affects the analysis of the stress gradient over the range of $\sin^2\psi=0\sim0.8$. For film thickness $t=200$ $\mu$m, $W_t$ is equal to $T$; thus, the effect of film thickness disappears. In a previous study[9], we reported that the thickness effect could be disregarded when the thickness is about six times larger than the effective X-ray penetration depth. This agrees with the calculated results shown in Fig. 4.

For the X-ray stress analysis of thin films, it is important to clarify the effect of film thickness on the $\sin^2\psi$ diagram. Firstly, we simulate the effect of the thickness of the films with the same stress distribution from the surface. The simulation results for several film thicknesses are shown in Fig. 5. The films have the same stress distribution, but the $\sin^2\psi$ diagram is different as shown in the figure. $\sin^2\psi$ of the thin film is affected by film thickness; therfore, we must use the analytical method where film thickness is taken into account. Since the stress difference in a 10-$\mu$m-thick film is small, nonlinearity of the $\sin^2\psi$ diagram becomes small. The difference in stress values of thicker films is large, and hence nonlinearity of the $\sin^2\psi$ diagram becomes considerable.

Figure 6 shows the results of the simulation of the $\sin^2\psi$ diagram for a film specimen with 50 $\mu$m thickness bent to various curvatures. From Eq.(24) and $A_2=\nu A_1$, Eq.(11) is rewritten as follows:

$$\langle 2\theta_{\phi=0\psi}\rangle=-\frac{2(1+\nu)}{E}\tan\theta_0(\sigma_{10}+A_1W_t)\sin^2\psi+\frac{2(1+\nu)\nu}{E}\tan\theta_0(\sigma_{10}+A_1W_t)+2\theta_0. \quad (25)$$

The $\langle 2\theta_{\phi=0\psi}\rangle$ value is equal to the stress-free diffraction angle $2\theta_0$ at $\sin^2\psi=\nu$, so the curves merge at $\sin^2\psi=\nu$. When we apply several values of the bending stress to the thin film, we have

$$\sin^2\psi=\nu,\quad \langle 2\theta_{\phi=0\psi}\rangle=2\theta_0 \quad (26)$$

$$\sin^2\psi=0,\quad \langle 2\theta_{\phi=0\psi}\rangle=\frac{2(1+\nu)\nu}{E}\tan\theta_0(\sigma_{10}+A_1W_t)+2\theta_0. \quad (27)$$

If the mechanical elastic constants are known, $\sigma_{10}$ and $A_1W_t$ can be calculated and then the X-ray elastic constants can be determined using Eqs.(26) and (27).

Our method of X-ray stress gradient analysis can be applied to ceramic film and other thin films. Since thin films are usually multi-layered rather than single-layered, the stress gradient analysis is important, in

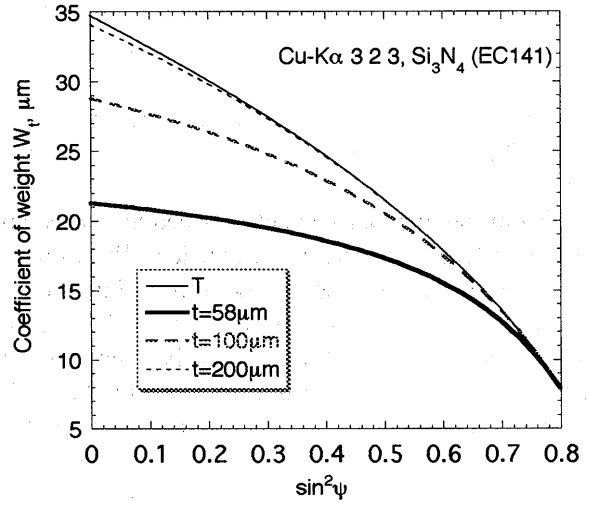


Fig. 4 Change in coefficient of weight with $\sin^2\psi$

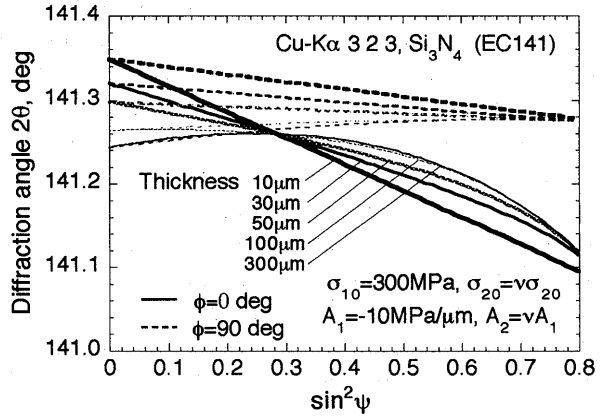


Fig. 5 Effect of film thickness on $2\theta$-$\sin^2\psi$ diagram

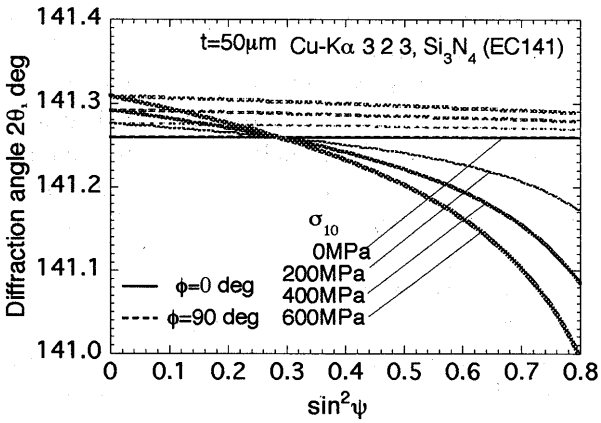


Fig. 6 Thin film with applied bending stresses

addition to the stress on the surface.

## 5. Conclusion

In the present study, we analyzed the stress gradients in ceramic thin film by taking into account the effect of film thickness. We assumed that the diffraction intensity from the entire thickness influences the stress analysis, and proposed the method of stress gradient analysis using the weighted coefficient including the the film thickness. We also derived a method for determining the parameters for stress distributions.

We applied our method to analysis of the stress gradient in the case of bending of a 58-$\mu$m-thick silicon nitride film. The analytical results agreed very well with applied stress distributions. It is concluded that the stress gradients should be determined from the weighted average stress over the entire thin film.

Under a given stress distribution, the nonlinearity of the $\sin^2\psi$ diagram becomes pronounced with an increase in film thickness, since the stress difference within the film is large. If the film thickness is six times larger than the effective X-ray penetration depth, the $\sin^2\psi$ diagram of the film corresponds to that of the bulk specimen. We also proposed a measurement method of X-ray elastic constants of the thin film by applying bending stresses.

## Acknowlegdement

This work was financially supported by a Grant-in-Aid for Science Research from the Ministry of Education, Sports, Science and Culture of Japan.

## References

(1) Chen, P. C. and Oshida, Y., Residual Stress Analysis of a Muti-Layer Thin Film Structure by Destructive (Curvature) and Non-Destuctive (X-ray) Method, Mat. Res. Soc. Symp. Proc., Vol. 153 (1989), p. 363.

(2) Oshida, Y. and Chen, P. C., Nondestructive Low-Cycle Fatigue Characterization of Multi-Layer Thin Film Structure, J. Nondestr. Eval., Vol. 8, No. 4 (1989), p. 235.

(3) Eigenmann, B., Scholtes, B. and Macherauch, E., X-ray Residual Stress Determination in Thin Chromium Coatings on Steel, Surface Eng., Vol. 7, No. 3 (1991), p. 221.

(4) Idemitsu, K., Endoh, T. and Kawakami, M., X-ray Measurement of Residual Stress Distribution in Later Heat Treated TiN Coated Caron Steels, Nondestr. Test Eval., Vol. 8, No. 9 (1992), p. 919.

(5) Durand, N., Badawi, K. F., Declemy, A. and Goudeau, Ph., Origin of Residual Stress in a Textured Au Thin Film on a LiF Substrate, Appl. Surface Sci., Vol. 81 (1994), p. 191.

(6) Shibano, J., Ukai, T., Tadano, S. and Todoh, M., Residual Stress Evaluation in the Vicinity of Ceramic Coating Interface Using Polychromatic X-ray Method, Trans. Jpn. Soc. Mech. Eng. (in Japanese), Vol. 61, No. 586, A (1995), p. 1356.

(7) Noyan, I. C., Huang, T. C. and York, B. R., Residual Stress/Strain Analysis in Thin Films by X-ray Diffraction, Critical Reviews in Solid State and Materials Sciences, Vo. 20, No. 2 (1995), p. 125.

(8) Yoshioka, Y., Sasaki, T. and Kuramoto, M., Multiaxial Stress Analysis Taking Account of Penetration Depth of X-rays, J. Soc. for Non-destructive Inspection, Jpn (in Japanese), Vol. 34 (1985), p. 52.

(9) Suzuki, K., Tanaka, K. and Sakaida, Y., Penetration Depth in X-ray Analysis of Steep Stress Gradient Near Surface, J. Soc. Mater. Sci., Jpn, (in Japanese), Vol. 45 (1996), p. 759.

(10) Sasaki, T., Kuramoto, M. and Yoshioka, Y., X-ray Stress Measurement in Zn-Ni Alloy Electroplating, The 26th Symp. on X-ray Studies an Mech. Behavior of Mater., Soc. Mater. Sci., Jpn, (in Japanese), (1989), p. 134.

(11) Sasaki, T., Kuramoto, M. and Yoshioka, Y., A Method of X-ray Tri-axial Stress Analysis for Thin Films and Example of its Application, J. Soc. for Non-destructive Inspection, Jpn (in Japanese), Vol. 42 (1993), p. 237.

(12) Sasaki, T. and Hirose, Y., A Method of X-ray Stress Measurement for Composite Materials Considering Macro- and Microstresses with Steep Stress Gradient, Trans. Jpn. Soc. Mech. Eng. (in Japanese), Vol. 61, No. 585, A (1995), p. 1031.

(13) Wolfstieg, U., $\psi$-Goniometer, HTM, Vol. 31 (1976), p. 19.

(14) Marquardt, D. W., An Algorithm for Least-Squares Estimation of Non-linear Parameers, J. SIAM, Vol. 11, No. 2 (1963), p. 431.

(15) Tanaka, K., Hattori, Y. and Tanaka, H., Diffraction-Plane Dependence of Elastic Constants of Silicon Nitride for X-ray Stress Measurement, J. Soc. Mater. Sci., Jpn (in Japanese), Vol. 44 (1995), p. 1110.